Energy Storage

International Edition: DOI: 10.1002/anie.201511452
German Edition: DOI: 10.1002/ange.201511452

Enhanced Pseudocapacitance in Multicomponent Transition-Metal Oxides by Local Distortion of Oxygen Octahedra

Hyeon Jeong Lee[+], Ji Hoon Lee[+], Sung-Yoon Chung, and Jang Wook Choi**

Abstract: *Anomalously high pseudocapacitance of a metal oxide was observed when Ni, Co, and Mn were mixed in a solid solution. Analysis by X-ray absorption near-edge spectroscopy (XANES) identified a wider redox swing of Ni as the origin of the enlarged pseudocapacitance. Ab initio DFT calculations revealed that aliovalent species resulting from the copresence of multiple transition metals can generate permanent local distortions of [NiO_6] octahedra. As this type of distortion breaks the degenerate e_g level of Ni^{2+}, the Jahn–Teller lattice instability necessary for the $Ni^{2+/3+}$ redox flip can be effectively diminished during charge–discharge, thus resulting in the significantly increased capacitance. Our findings highlight the importance of understanding structure–property correlation related to local structural distortions in improving the performance of pseudocapacitors.*

As pseudocapacitors store charge on the basis of dual ("faradaic" and "capacitive") modes, they have advantages for both rechargeable batteries and ultracapacitors.[1] While a long cycle life and high rate performance are feasible with a nondestructive capacitive storage mechanism, the energy density can be boosted by faradaic charge transfer into the active bulk material.[2] One of the main directions in pseudocapacitor research in the past decade has been the integration of nanostructured metal oxides, hydroxides, and chalcogenides with conductive carbon nanomaterials,[3] such as graphene and carbon nanotubes. Nanostructures bring the benefits of high rate capability as well as long cycle life related to the improved mechanical stability of active phases, as nanomaterials are better at releasing strain. The nanostructure effect of metal oxides has been verified for a variety of morphologies with diverse transition metals (TMs), such as Ni, Co, Mn, Fe and V.[4] Nonetheless, a majority of studies have focused solely on nanostructure effects, and the impact of the choice of TM or the mixing of multiple TMs on electrochemical performance has not been examined in depth.

In this study, we have systematically investigated the impact of multiple TMs, particularly those commonly adopted as pseudocapacitor active materials: Ni, Co, and Mn. Interestingly, when the three TMs were mixed in equal amounts, the specific capacitance rose far beyond those observed with the individual TMs, thus indicating a synergistic effect of TM mixing. Combined experimental and theoretical analysis revealed that the enhanced performance originates from permanent local distortions of [NiO_6] octahedra in the presence of aliovalent cations (Co^{3+} and Mn^{4+}) and transition-metal vacancies (V_M), among which V_M has the largest effect on distorting the nearest neighboring [NiO_6] octahedra. The degenerate e_g level in Ni^{2+}, the primary redox center for capacitance acquisition, is split through this permanent distortion, thus enabling the energetically more facile redox swing of $Ni^{2+/3+}$ by alleviating the structural variation from a Jahn–Teller effect.[5]

To investigate the effect of mixing the three TMs, we adopted the known procedure of dispersing $M(CH_3COO)_2{\cdot}4H_2O$ (M = Ni, Co, Mn) in a solution of graphene oxide (GO). The GO solution containing the precursors was reduced by the addition of hydrazine hydrate ($NH_2NH_2{\cdot}H_2O$) at 72 °C under reflux conditions.[6] The resultant blackish powder was further thermally treated to produce mixed-transition-metal-oxide nanoparticles (NPs) supported on reduced graphene oxide (rGO); this material is referred to herein as MixO-rGO (Figure 1a; see the Supporting Information for details). Other individual MO-rGO (M = Ni, Co, and Mn) samples used as controls were prepared by the same procedure. The metal-oxide content in each sample was approximately 45 % by weight (see Figure S1 in the Supporting Information).

According to the X-ray diffraction (XRD) pattern (Figure 1b), MixO-rGO has a rocksalt structure with the space group *Fm*-3*m*. The sharp peak at approximately 23° originates from rGO.[7] The peaks of MixO-rGO do not split into individual peaks corresponding to each TM oxide (reference peaks are shown below the XRD pattern of MixO-rGO) but rather appear broader. These broadened peak shapes are attributed to solid-solution mixing of the three TMs as well as the small sizes of NPs. Transmission electron microscopy (TEM) images (Figure 1c,d) show decent dispersion of MixO NPs. The TEM analysis results are in good agreement with the above XRD results; a high-resolution (HR) image (Figure 1d, top inset) shows lattice fringes with interlayer distances of 2.46 and 2.10 Å assigned to the (111) and (200) lattice orientations in the rocksalt structure, respectively. The fast Fourier transform (FFT) pattern (Figure 1d, bottom inset) of the HRTEM image contains spots consistent with the lattice orientations observed. The uniform distribution of NPs was also reflected by a scanning transmission electron microscope (STEM) image, whose elemental mapping verifies

[*] H. J. Lee,[+] J. H. Lee,[+] Prof. S.-Y. Chung, Prof. J. W. Choi
Graduate School of EEWS and KAIST Institute NanoCentury
Korea Advanced Institute of Science and Technology (KAIST)
291 Daehak-ro, Yuseong-gu, Daejeon 34141 (Republic of Korea)
E-mail: sychung@kaist.ac.kr
jangwookchoi@kaist.ac.kr

[+] These authors contributed equally to this work.

Supporting information for this article can be found under http://dx.doi.org/10.1002/anie.201511452.

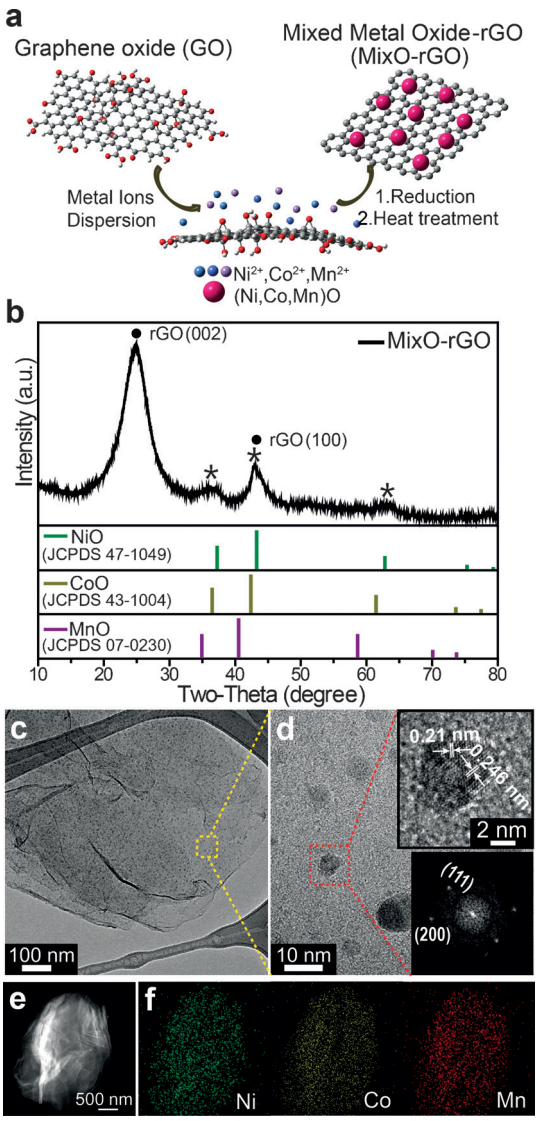

Figure 1. a) Synthetic route to the mixed metal oxide supported on reduced graphene oxide (MixO-rGO). b) XRD pattern of as-prepared MixO-rGO. c) TEM image of MixO-rGO. d) HRTEM image of crystalline MixO nanoparticles magnified from the yellow box in (c). The insets show lattice fringes and the FFT pattern of the nanoparticle in the red box. e) STEM image of MixO-rGO. f) Element mapping for the nanoparticles shown in (e) with respect to Ni, Co, and Mn.

homogeneous distribution with respect to each TM (Figure 1e,f).

The electrochemical performance of the MO-rGO series was evaluated under a three-electrode configuration. The stable electrochemical window was first determined by using a blank Pt electrode (see Figure S2). An oxygen-evolution reaction (OER) was detected above 0.6 V versus Hg/HgO when measured at 10 $mV s^{-1}$. To exclude capacitance contributed by a current collector, we used conductive carbon paper.[8] The carbon paper showed inert electrochemical behavior in the given voltage window, in contrast with a Ni plate, which underwent repeated phase transitions (see Figure S3). Under a three-electrode configuration, MixO-rGO exhibited conspicuous plateaus in galvanostatic measurements (Figure 2a). As clearly revealed by the galvanostatic measurements at the same current density of 2 $A g^{-1}$ in Figure 2b, the MixO-rGO electrode showed remarkably higher capacitances at all current densities as compared to those of any individual MO-rGO counterparts (Figure 2c; see also Figure S4). For example, at a low current density of 2 $A g^{-1}$, MixO-rGO, NiO-rGO, and CoO-rGO delivered 510, 330, and 106 $F g^{-1}$, respectively. Also, the redox voltages of MixO-rGO support its solid-solution behavior from the participating TMs; instead of three discrete plateaus, MixO-rGO showed one steep plateau (or broader peak in the CV measurement) during each charge and discharge process (Figure 2a; see Figure S5a). Its equilibrium redox potential of approximately 0.35 V (vs. Hg/HgO), which is an intermediate value between those (ca. 0.41 and ca. 0.18 V (vs. Hg/HgO)) of NiO-rGO and CoO-rGO, is another indication of the solid-solution behavior (see Figure S5a–c). In contrast with the other samples, MnO-rGO showed no redox activity (see Figure S5d), thus indicating that when solely used, MnO is inactive in basic electrolytes. Furthermore, NiO-rGO exhibited a poor cycle life, which might result from a combination of the partial dissolution of NiO and the oxygen-evolution reaction (OER).[9] In contrast, the redox process with MixO-rGO appears very robust, as 93.4% of the initial capacitance was retained after 1500 cycles when it was cycled at 4 $A g^{-1}$ (Figure 2d).

To evaluate the contribution to the obtained capacitance from rGO, we performed an electrochemical test for bare rGO under the same conditions (see Figure S6). From the galvanostatic measurement, the specific capacitance of rGO was determined to be approximately 40 $F g^{-1}$. Therefore, the capacitance from the series of MO-rGO is accounted for mainly by the pseudocapacitance of the TM oxides. The superior capacitances of MixO-rGO as compared with those of the other individual MO-rGOs are indeed quite surprising because when TMs are mixed, the properties of MixO-rGO are expected to be an average of those observed for the individual MO-rGOs. The observed phenomenon is particularly remarkable, as Mn, which accounts for one-third of all TMs, turned out to be inactive in the electrochemical measurement of MnO-rGO. In another control experiment (see Figure S7), MixO-rGO exhibited better performance than $Ni_{0.5}Co_{0.5}O$-rGO, thus implying the critical role of Mn in our material containing three TM components, although it is inactive itself.

In an effort to identify the effect of multicomponent TMs, we carried out X-ray absorption near-edge structure (XANES) analysis for MixO-rGO and its individual MO-rGO counterparts at different charging and discharging states (Figure 3). The redox states of the TMs identified by XANES analysis provide useful information on the electrochemical properties of each electrode, and the following three points are especially notable. First, MixO-rGO shows larger redox swing ranges at the Ni K-edge (Figure 3a,d) and Co K-edge (Figure 3b,e) than the individual MO-rGOs, which must be the origin of the higher capacitances of MixO-rGO. Second, by contrast, at the Mn K-edge (Figure 3c,f), the Mn redox state in MixO-rGO starts at a position closer to 3+ and shifts to 4+ in the first charge process. After that, its oxidation state

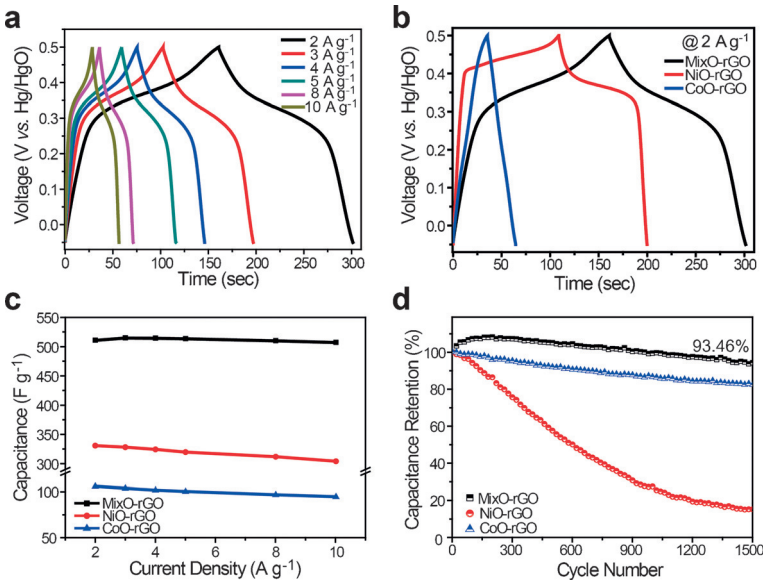

Figure 2. a) Galvanostatic charge/discharge curves of MixO-rGO at various current densities from 2 to 10 A g^{-1}. b) Comparative galvanostatic charge/discharge curves at a current density of 2 A g^{-1} and c) capacitance changes of the materials at different current densities. d) Cycle lives of the three samples.

remains unchanged during the remaining charge–discharge cycles. Distinct from this behavior, the Mn redox state in MnO-rGO never shifts at all from the pristine state near 2+ in all electrochemical processes in the alkaline medium. The almost inactive or completely inactive nature of the Mn redox center is ascribed to the well-known Jahn–Teller effect[5] of Mn^{3+}; the oxidation-state change of Mn from 2+ or 4+ to 3+ imposes a substantial structural barrier for the development of strain. Finally, the oxidation states of the TMs are distinct between MixO-rGO and the individual MO-rGO materials in the pristine states. The oxidation state of all the individual MO-rGO samples is consistently 2+. By contrast, the Ni, Co, and Mn in MixO-rGO start at oxidation states near 2+, 2+, and 3+, respectively. From this ionic-size viewpoint,[10] the ionic radius (83 pm) of Mn^{2+} is significantly larger than those of Ni^{2+} (69 pm) and Co^{2+} (75 pm); thus, Mn^{3+} with a similar size (65 pm) may be preferred in the MixO framework. The formation of Mn^{3+} would, in turn, yield V_M to satisfy charge neutrality.[11] In the case of pristine MnO-rGO, to generate an oxidation state of 2+ in analogy with the other TM controls, we heat-treated the sample at 800 °C.

The combined XANES and electrochemical results led to the speculation that the enhanced capacitance of MixO-rGO could be attributed to physicochemical environmental changes due to the solid-solution mixing of TMs. In an attempt to unveil such an anomalous phenomenon, we carried out density functional theory (DFT) calculations.

Comparison of the XANES spectra at the different TM edges for MixO-rGO indicated that MixO-rGO experiences a much wider redox swing for Ni than for Co and Mn (Figure 3 a–c). This observation indicates that the oxidation-state change of Ni mostly accounts for the observed capaci-

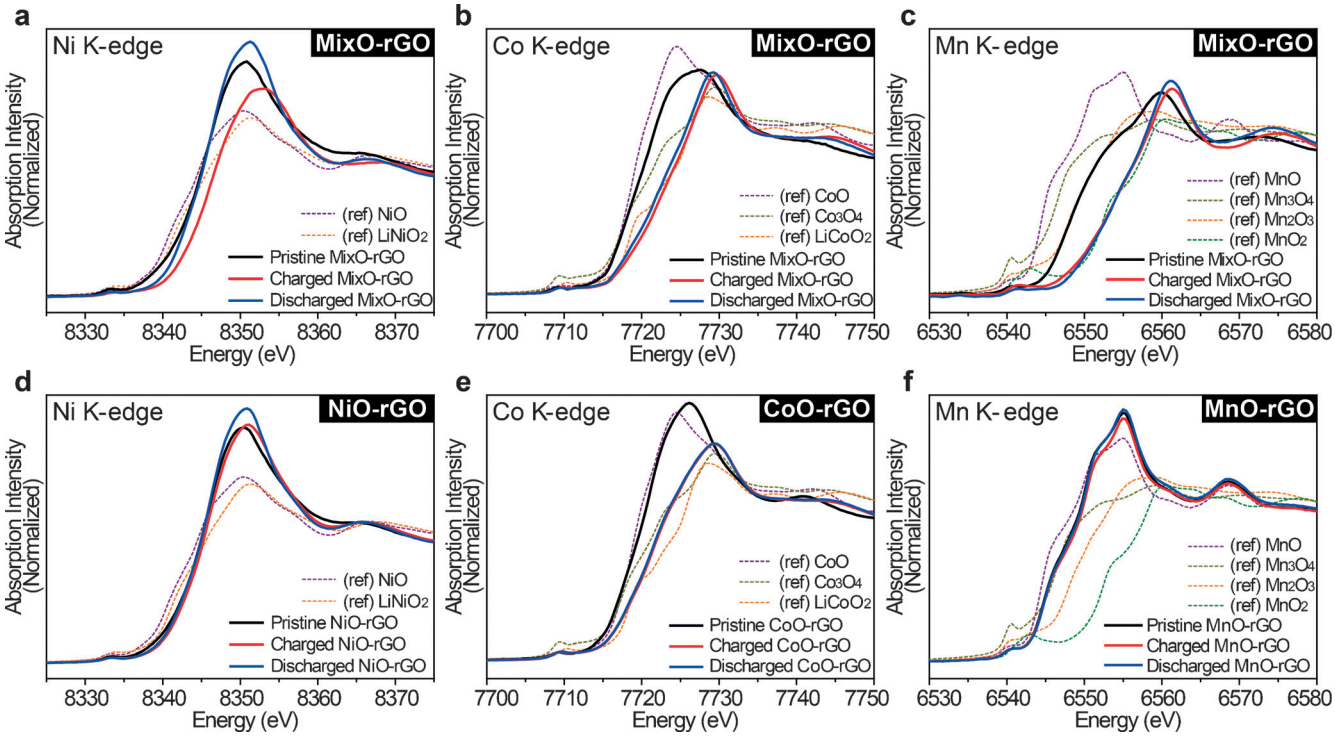

Figure 3. XANES spectra of the mixed and pure metal oxides in the pristine, charged, and discharged states: a–c) Ni K-edge, Co K-edge, and Mn K-edge profile of MixO-rGO, respectively. d) Ni K-edge profile of NiO-rGO. e) Co K-edge profile of CoO-rGO. f) Mn K-edge profile of MnO-rGO.

tance of MixO-rGO. Accordingly, in the DFT calculation, we set a NiO unit cell as a structural platform to see how its geometry optimization would be affected by the series of aliovalent species (Co^{3+}, Mn^{4+}, and V_M). In the perfect NiO unit cell after geometric optimization (Figure 4a), every [NiO_6] octahedron had an identical Ni–O interatomic distance of 2.077 Å. In contrast, when other species were introduced, it was observed that the Ni–O bond length deviated from that in the perfect NiO unit cell. First, to reflect the sequential electrochemical reaction in MixO-rGO (see Figure S5b,c), we substituted one Co^{3+} ion into a [NiO_6] octahedron (Figure 4b). In this case, the optimized unit cell showed a reduced Ni–O interatomic distance of 2.028 Å for the [NiO_6] octahedron adjacent to Co^{3+}. This result implies that the introduction of the aliovalent species can bring a permanent distortion of the nearest neighboring [NiO_6] octahedra. Interestingly, such a local distortion becomes more remarkable with Mn^{4+} and V_M, as their adjacent Ni–O bond lengths are reduced to 2.000 and 1.853 Å, respectively (Figure 4c,d). The series of geometric optimization confirms that the local distortion of [NiO_6] octahedra can be induced in the MixO matrix in a permanent way, and these distortions turn out to be more significant in the order $V_M > Mn^{4+} > Co^{3+}$, as confirmed from the nearest neighboring Ni–O interatomic distances.

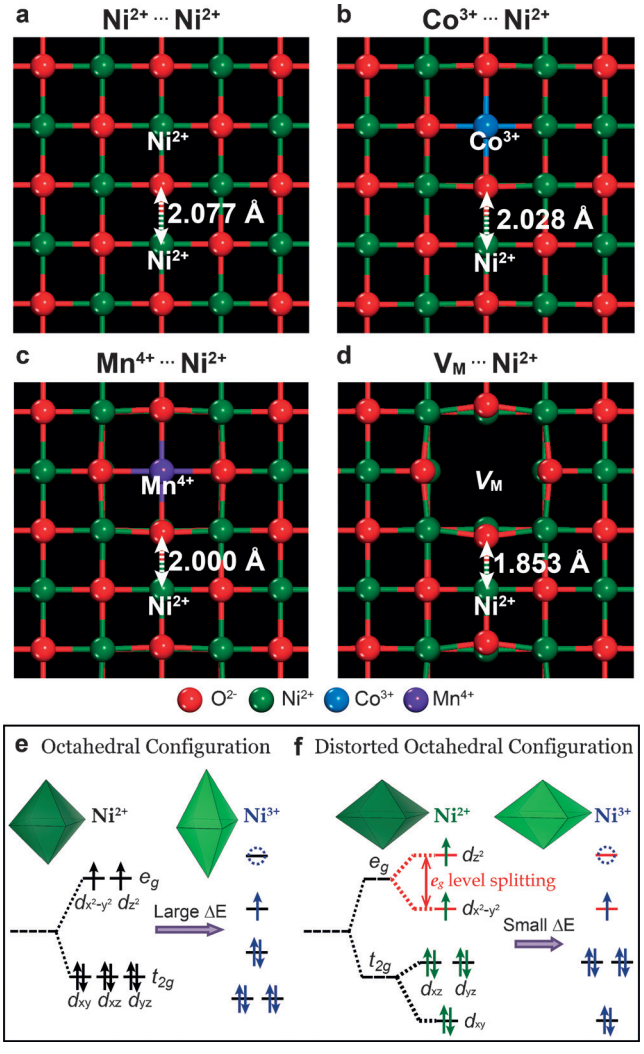

Figure 4. Geometrically optimized unit-cell configurations for a) perfect NiO and b–d) NiO with various aliovalent species: Co^{3+} (b), Mn^{4+} (c), and V_M (d). e,f) Schematic description of the 3d orbital configurations for the octahedral (e) and distorted octahedral fields (f), which correspond to (a) and (b–d), respectively.

To elucidate the origin of the enlarged $Ni^{2+/3+}$ redox swing of MixO-rGO, it is necessary to explain the smaller $Ni^{2+/3+}$ redox swing of NiO-rGO. According to crystal field theory,[12] the 3d orbitals of a TM octahedron typically have an octahedral field configuration with the orbitals split into the degenerate e_g and t_{2g} levels (Figure 4e). Octahedrally coordinated Ni^{2+} has a $3d^8$ orbital with an electronic configuration of $t_{2g}^6 e_g^2$. However, during charging, NiO-rGO undergoes Jahn–Teller distortion due to the low-spin Ni^{3+} ions ($t_{2g}^6 e_g^1$),[5,13] thus implying that a significant structural strain and subsequent lattice instability are induced during the electrochemical reaction. Distinct from this behavior, in the case of MixO-rGO, each [NiO_6] octahedron is "predistorted" by the neighboring aliovalent species (Figure 4b–d), as revealed by the geometry optimization from DFT calculations. Therefore, the degeneracy of the e_g level is broken as a result of the different ligand effect of each oxygen atom, and a distorted octahedral field configuration is allowed even for a [$Ni^{2+}O_6$] octahedron (Figure 4f). Consequently, unlike the case of NiO-rGO, MixO-rGO does not need to undergo the significant Jahn–Teller distortion for Ni^{3+}, thus remarkably alleviating the structural variation during the electrochemical reaction. Also, considering the theoretical results, V_M has the largest effect on reducing the interatomic distance of Ni–O, by approximately 10% (from 2.077 to 1.853 Å), for the neighboring [NiO_6] octahedron; thus, it can be deduced that V_M plays the most important role in enhancing the redox flip of $Ni^{2+/3+}$ in MixO-rGO. The facilitated redox reaction of MixO-rGO was also verified by electrochemical measurements, in which the limiting step was identified between charge transfer and bulk diffusion (see Figure S8).

In conclusion, this study introduces a new opportunity to improve the electrochemical performance of pseudocapacitors through the mixing of multiple TM cations. The solid-solution mixing of multiple TMs predistorts the framework and consequently mitigates Jahn–Teller-type structural variation during the redox reaction, thus resulting in a significantly wider redox swing of Ni and larger pseudocapacitance of the solid solutions. The findings of this study demonstrate the importance of structure–property relationships in the design and improvement of key active materials in emerging energy-storage systems.

Acknowledgements

We acknowledge support by National Research Foundation of Korea (NRF) grants funded by the Korean government (MEST; NRF-2012-R1A2A1A01011970 and NRF-2014R1A4A1003712). We also acknowledge technical support with the 7D beamline (X-ray adsorption fine structure; XAFS) at PAL.

Keywords: electrochemistry · Jahn–Teller distortion · octahedron distortion · pseudocapacitors · solid solutions

How to cite: *Angew. Chem. Int. Ed.* **2016**, *55*, 3958–3962
Angew. Chem. **2016**, *128*, 4026–4030

[1] P. Simon, Y. Gogotsi, *Nat. Mater.* **2008**, *7*, 845–854.
[2] Z. G. Yang, J. L. Zhang, M. C. W. Kintner-Meyer, X. C. Lu, D. W. Choi, J. P. Lemmon, J. Liu, *Chem. Rev.* **2011**, *111*, 3577–3613.
[3] a) G. Yu, L. Hu, N. Liu, H. Wang, M. Vosgueritchian, Y. Yang, Y. Cui, Z. Bao, *Nano Lett.* **2011**, *11*, 4438–4442; b) H. L. Wang, H. S. Casalongue, Y. Y. Liang, H. J. Dai, *J. Am. Chem. Soc.* **2010**, *132*, 7472–7477; c) G. A. Muller, J. B. Cook, H.-S. Kim, S. H. Tolbert, B. Dunn, *Nano Lett.* **2015**, *15*, 1911–1917.
[4] a) Q. Lu, J. G. G. Chen, J. Q. Xiao, *Angew. Chem. Int. Ed.* **2013**, *52*, 1882–1889; *Angew. Chem.* **2013**, *125*, 1932–1940; b) H. Wang, J. T. Robinson, G. Diankov, H. Dai, *J. Am. Chem. Soc.* **2010**, *132*, 3270–3271; c) Z.-S. Wu, W. Ren, D.-W. Wang, F. Li, B. Liu, H.-M. Cheng, *ACS Nano* **2010**, *4*, 5835–5842; d) Q. Qu, Y. Zhu, X. Gao, Y. Wu, *Adv. Energy Mater.* **2012**, *2*, 950–955.
[5] a) H. A. Jahn, E. Teller, *Proc. R. Soc. A*, **1937**, *161*, 220–235; b) J. E. Huheey, E. Keiter, R. Keiter, *Inorganic Chemistry: Principles of Structure and Reactivity*, 4th ed., Harper Collins College Publishers, New York, **1993**.
[6] S. Stankovich, D. A. Dikin, R. D. Piner, K. A. Kohlhaas, A. Kleinhammes, Y. Jia, Y. Wu, S. T. Nguyen, R. S. Ruoff, *Carbon* **2007**, *45*, 1558–1565.
[7] J. H. Lee, N. Park, B. G. Kim, D. S. Jung, K. Im, J. Hur, J. W. Choi, *ACS Nano* **2013**, *7*, 9366–9374.
[8] W. Xing, S. Z. Qiao, X. Z. Wu, X. L. Gao, J. Zhou, S. P. Zhuo, S. B. Hartono, D. Hulicova-Jurcakova, *J. Power Sources* **2011**, *196*, 4123–4127.
[9] J. B. Wu, Z. G. Li, Y. Lin, *Electrochim. Acta* **2011**, *56*, 2116–2121.
[10] R. D. Shannon, *Acta Crystallogr. Sect. A* **1976**, *32*, 751–767.
[11] R. J. D. Tilley, *Defects in Solids*, Wiley, Hoboken, **2008**, pp. 1–44.
[12] J. H. Van Vleck, *Phys. Rev.* **1932**, *41*, 208–215.
[13] I. Nakai, T. Nakagome, *Electrochem. Solid-State Lett.* **1998**, *1*, 259–261.

Received: December 10, 2015
Published online: February 17, 2016

